Chem. Res. Chinese Universities, 2020, 36(1), 10—23 doi: 10.1007/s40242-020-9068-7

Review

Recent Advances in Two-dimensional Materials for Electrochemical Energy Storage and Conversion

YANG Chao[1,2], WANG Hao-Fan[1] and XU Qiang[1*]

1. AIST-Kyoto University Chemical Energy Materials Open Innovation Laboratory(ChEM-OIL), National Institute of Advanced Industrial Science and Technology(AIST), Yoshida, Sakyo-ku, Kyoto 606-8501, Japan;

2. School of Materials Science, Japan Advanced Institute of Science and Technology, 1-1 Asahidai, Nomi 923-1292, Japan

Abstract With the increased energy demand, developing renewable and clean energy technologies becomes more and more significant to mitigate climate warming and alleviate the environmental pollution. The key point is design and synthesis of low cost and efficient materials for a wide variety of electrochemical reactions. Over the past ten years, two-dimensional(2D) nanomaterials that graphene represents have been paid much attention as a class of the most promising candidates for heterogeneous electrocatalysts in electrochemical storage and conversion. Their unique properties, such as good chemical stability, good flexibility, and good electronic properties, along with their nano-sized thickness and large specific area, make them exhibit comprehensively good performances for energy storage and conversion. Here, we present an overview on the recent advances in electrochemical applications of graphene, graphdiyne, transition metal dichalcogenides(TMDs), and MXenes for supercapacitors(SCs), oxygen reduction reaction (ORR), and hydrogen evolution reaction(HER).

Keywords Two-dimensional material; Graphene; Graphdiyne; Layered transition-metal dichalcogenide; MXene; Energy storage and conversion

1 Introduction

In the last decade, various 2D nanomaterials, such as graphene[1], graphdiyne[2], transition metal dichalcogenides (TMDs)[3], MXenes[4], hexagonal boron nitride(hBN)[5], graphitic carbon nitride(g-C_3N_4)[6], layered double hydroxides (LDHs)[7], metals[8], metal-organic frameworks(MOFs)[9], covalent organic frameworks(COFs)[10], polymers[11], black phosphorus(BP)[12], and perovskite[13] have been applied in many fields, especially for energy storage and conversion[14—20]. In order to obtain 2D monolayers, a variety of methods have been developed[21—24]. Besides the most well-known method-micromechanical cleavage[25], in which the high quality 2D materials are produced for exploring some important physical phenomena and excellent device performance, most of 2D monolayers can be obtained by top-down methodology since the anisotropy of layered bulks makes the interlayered interaction weaker than the strong in-plane covalent bonds[26—29]. In addition, the interlayered interaction can be reduced by enlarging interlayered distance using intercalator and/or changing

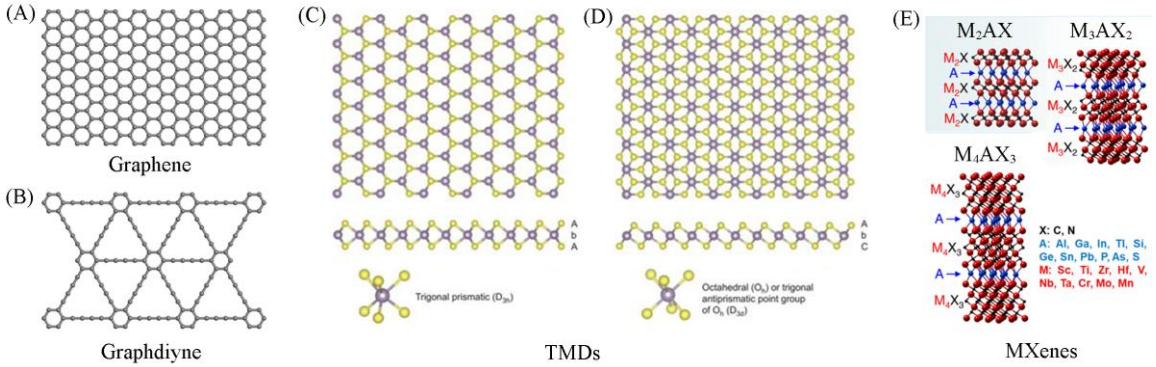

Fig.1 Fundamental structures and distinctive characteristics of graphene(A), graphdiyne(B), TMDs with trigonal prismatic(C), and octahedral coordinations(D) and MXenes(E)

Reprinted with permission from: (C) and (D) Ref. [3], Copyright 2013, Nature Publishing Group; (E) Ref. [29], Copyright 2017, Nature Publishing Group.

*Corresponding author. Email: q.xu@aist.go.jp

Received November 27, 2019; accepted December 26, 2019.

Supported by the Project of National Institute of Advanced Industrial Science and Technology of Japan(AIST) and China Scholarship Council(CSC).

the circumstance inside or outside monolayers *via* chemical transformation. This enables efficiently spontaneous exfoliation or external force(like sonication, shear, microwave, and so on) assisted exfoliation in liquid phase[30—34]. Meanwhile, bottom-up methods like chemical vapor deposition(CVD) have become more and more important for the synthesis of high-crystallinity, high-purity, and low-defect 2D nanomaterials and their alloys[35—38]. In this review, features and advantages of four representative 2D inorganic nanomaterials, including graphene, graphdiyne, TMDs, and MXenes are firstly summarized(Fig.1). Then the applications of these 2D nanomaterials for supercapacitors(SCs), oxygen reduction reaction(ORR), and hydrogen evolution reaction(HER) are introduced. Finally, we will provide some perspectives on the development of 2D materials for energy storage and conversion.

2 Features of 2D Nanomaterials

2.1 Graphene and Graphdiyne

2.1.1 Pristine Graphene and Graphdiyne

Graphene has become one of the most frontier research hot spots in electrochemistry, mainly due to its high theoretic surface area, high electrical conductivity, high electron transfer ratio, and high modulus of elasticity[39—42]. Compared with three-dimensional(3D) bulk graphite, π-π interaction between interlayers in graphene is prohibited, so that the perfect graphene has a thickness of only one carbon atom(0.34 nm), which brings unique properties, such as a high electrical conductivity of 10^6 S/cm[43]. By contrast of graphene comprised only sp^2-hybridized carbon atoms, graphdiyne is formed by the combination of *sp*- and sp^2-hybridized carbon atoms[44]. However, the lack of heteroatoms results in low intrinsic electrocatalytic activity. Therefore, modifications on graphene and graphdiyne by doping with heteroatoms or hybridizing with other active materials are necessary to activate graphene for energy storage and conversion[45—47].

2.1.2 Functionalized Graphene and Graphdiyne

The doping of heteroatoms into graphene realizes electron redistribution, polariton, and active defect sites because the size, electronegativity, and orbital hybridization of heteroatoms are different from those of carbon. Doped graphene often exhibits an enhanced electrochemical performance, which can be tuned by adjusting the doping mode, total dopant content, and doping procedure.

The nitrogen atom is the most common dopant for carbon materials including graphene because its size is similar to the carbon atom and its electronegativity is larger[48]. This means the electronic/ionic conductivity of nitrogen-doped graphene will be enhanced due to the higher electronegativity of nitrogen (3.04), leading to more electrons attracted toward the doped region[49].

The boron atom can be in-plane doped into graphene by sp^2 hybridization, which retains the planar structure of graphene without distortion[50]. The relatively greater electropositivity between boron and carbon atoms enables charge polarization in graphene due to one less valence electron to the neighboring carbon, stabilizing the negatively polarized atoms[51]. The sulfur atom has a very similar negativity(2.58) with that of the carbon atom(2.55), but its larger atomic size and polarizability result in higher spin density, edge strain, and charge delocalization[52]. In contrast with nitrogen, the electronegativity of phosphorus(2.19) is lower than that of carbon. Thus, the polarity of the C—P bonding is opposite to that of the C—N bonding. However, in phosphorus doped region, sp^3 hybridization is favorable because of the strong hybridization between P 3*p* and C 2*p* orbitals, giving rise to structural distortion, decreased conductivity and defects owing to the broken plane of graphene[53].

Edge-selectively halogenated graphene and in-plane halogenated graphene are achieved by doping with halogen. In halogenated graphene, the in-plane carbon atoms linked with halogens have sp^3 hybridization and the edged carbon atoms linked with halogens remain sp^2 hybridization[54]. Since the electronegativities of halogen atoms[fluorine(2.98), chlorine (3.16), bromine(2.96), iodine(2.66)] are larger than that of carbon atoms, they can also polarize adjacent carbon atoms. The band structure of halogenated graphene depends on the degree of halogenation[55,56].

Surface functionalization is a useful approach to enhance the electrochemical performance of graphene(Fig.2). The easiest and the most common way to functionalize graphene is preparing graphene oxide(GO), which has rich oxygen functional groups. However, GO usually exhibits poor charge storage performance due to its poor electrical conductivity. Effective pseudocapacitance will be achieved when GO is reduced to reduced GO(rGO) since the conjugated structure is partially recovered after reduction. Besides that, acylation, diazotization, cycloaddition reaction, esterification as well as noncovalent functionalization *via* π-π stacking and hydrophobic/philic interaction also can be used to modify the surface properties of graphene[57—62].

The outstanding electrical conductivity of graphdiyne is beneficial to energy storage and conversion[63]. In addition, some carbon atoms in graphdiyne are positively charged, resulting in an intrinsic electrocatalytic activity with a theoretical bandgap close to Si[64]. Due to the special structure of graphdiyne, for example, the *sp* hybridized carbon, its electronic performance can be modulated by the introduced site-specific pyridinic and *sp* hybridized N atoms, which are considered as the more beneficial active sites[65—68]. Moreover, doped graphdiyne with graphitic S and graphitic P is predicted theoretically to exhibit remarkable electroactivity[69]. It is indicated that the sp^2 hybridized C atom sites are more favorable than *sp* hybridized C atom sites to be doped with boron[70]. After fluorination or chlorination, both *sp* and sp^2 carbon atoms can be converted into the sp^3 carbon with elongated C—C bonds[71,72].

2.2 TMDs

TMDs are a class of important materials for energy storage and conversion[73—75]. Different from graphene, the monolayered TMDs can be described as a sandwich structure, where one layer of transition metals(M) is between two layers of

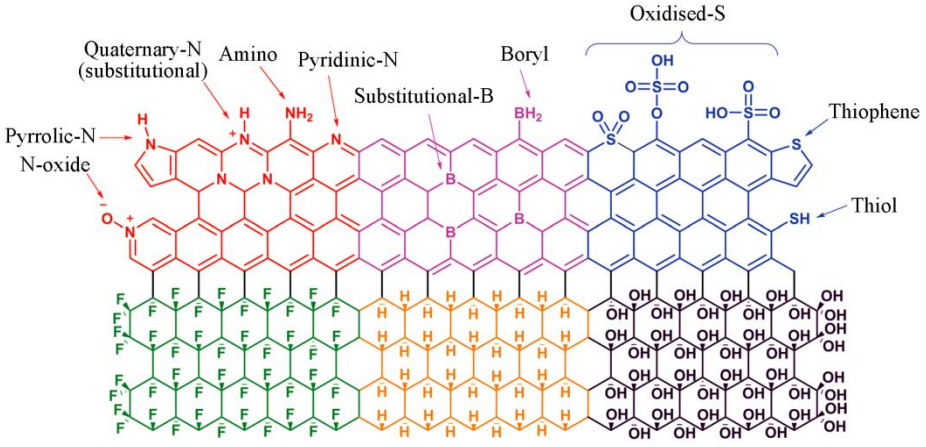

Fig.2 Illustrations of the structures of nitrogen-doped(red), boron-doped(pink), sulfur-doped(blue), fluorinated(green), hydrogenated(yellow), and hydroxylated(purple) graphene

Reprinted with permission from Ref. [62], Copyright 2016, Royal Society of Chemistry.

chalcogenides(X), rather than a perfect plane, resulting in a larger thickness. In some occasions, unlike graphene, TMDs are semiconductive due to the nonzero band gap[76]. However, since TMDs have different metal coordinations, they possess various multicrystal structures, such as 1T, 1H, 1T', 2H, and 3R(Fig.3), whose surface property and electronic performance are much instinct[77]. For example, the bandgap of 2H MoS_2 monolayers is 1.9 eV, while 1T MoS_2 is metallic with a bandgap of only 0.9 eV[78]. This is because that the bandgap for 2H phase is between d_{z^2} full band and $d_{x^2-y^2, xy}$ vacancy band, while a Fermi bandgap exists in $d_{xy, yz, xz}$ single band for 1T phase. In general, a metallic phase exhibits more active performance in energy conversion and storage[79].

CVD and lithium intercalation exfoliation are the most common methods to produce TMD monolayers[80,81]. Compared with CVD, lithium intercalation not only results in a nearly 100% yield of monolayers but also transforms 2H phase into 1T phase effectively[82,83]. However, an incomplete phase transformation is accompanied by this procedure so that 1T′ and 1T″ phases might exist. For 1T′ phase, the Mo atoms of MoS_2 become asymmetrically spaced with increased lithiation, which is shown to be energetically favorable compared to other possible polymorphs according to the DFT calculations[84]. Moreover, when TMDs are exfoliated into monolayers or thin sheets, the prismatic edges and basal planes are exposed, and edge termination by either M or X atoms is possible, which is recognized as the active site for electrocatalysis. Once the atom density in the nanosheets drops below a critical threshold size, the effects of the edge and corner atoms can dominate over the basal plane atoms, so that the equilibrium shape of the cluster can be controlled by modifying the edge atoms[85]. Other defects, such as vacancies, adatoms, grain boundaries, and substitutional impurities have been proved to play a significant role on the performance of TMDs in electrocatalysis[86].

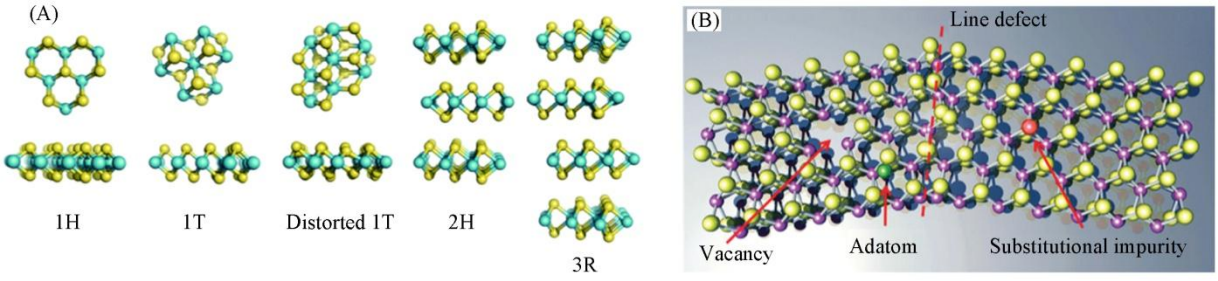

Fig.3 Structural polytypes of pristine TMD layers(A) and schematic illustration of the MoS_2 crystal structure with typical defects, including vacancy, adatom, substitutional impurity and line defects(B)

(A) Chalcogen atoms are shown in yellow, and transition metal atoms are shown in blue(1H, 1T phase, distorted 1T, or 1T′ and 2H phase). Reprinted with permission from Ref. [77](A) and Ref. [86](B), Copyright 2015 and 2018, respectively, Royal Society of Chemistry.

2.3 MXenes

MXenes are a new family of 2D materials since they were discovered in 2011 by Gogotsi and Barsoum *et al.*[87]. They are usually obtained from their layered precursors, such as MAX phases(Fig.4). MAX consists of $M_{n+1}X_n$(M_2X, M_3X_2 and M_4X_3) layers and planar A atomic sheets, where M is an early transition metal, such as scandium, titanium, zirconium, hafnium, vanadium, niobium, tantalum, chromium, molybdenum, manganese, and so on; A is a group IIIA or IVA element, such as aluminum, silicon, phosphorus, gallium, germanium, arsenic, and so on; and X is carbon or nitrogen[29,88]. In contrast to the weak van der Waals interactions between the layers of graphite and TMDs, the strong M—X bonds characterized by mixed covalent/metallic/ionic and metallic M—A bonds in MAX can hardly be broken by mechanical separation[89]. However, compared to the M—X bonds, the interlayered M—A bonds and interatomic A—A bonds are much weaker and more chemically

reactive. Thus, the A atomic layers from the parent MAX phase can be removed by hydrofluoric acid(HF) etching at room temperature. Afterwards, $M_{n+1}X_nT_x$ monolayers can be chemically terminated with oxygen, OH, and/or fluorine atoms on the surface, where T_x stands for the surface terminations[90—92].

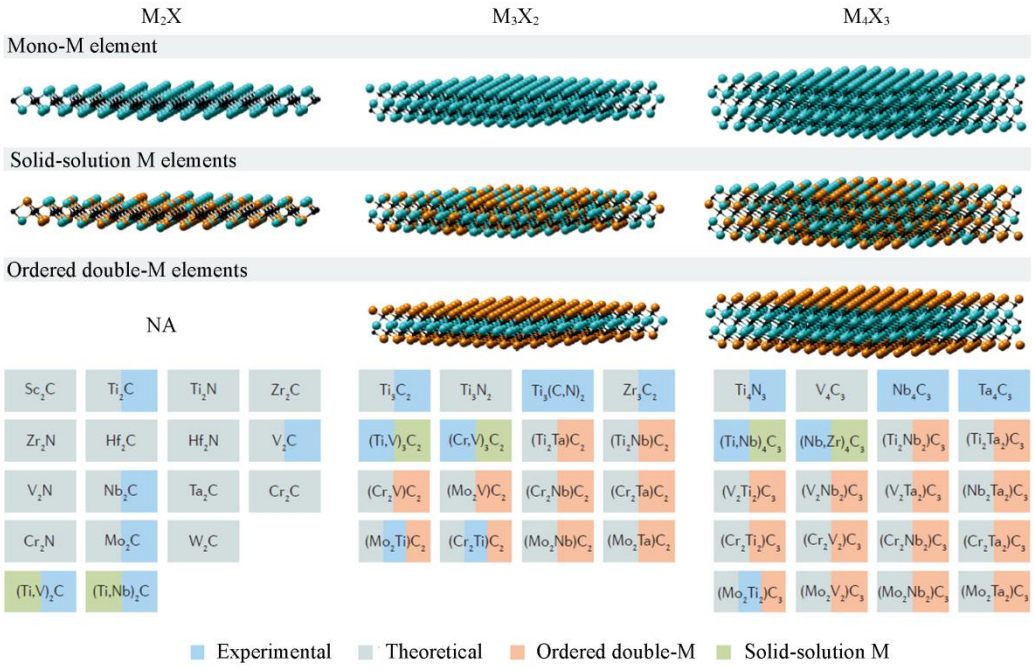

Fig.4 MXenes reported so far

MXenes can have at least three different formulas: M_2X, M_3X_2 and M_4X_3, where M is an early transition metal and X is carbon and/or nitrogen. They can be made in three different forms: mono-M elements(for example, Ti_2C and Nb_4C_3); a solid solution of at least two different M elements[for example, $(Ti,V)_3C_2$ and$(Cr,V)_3C_2$]; or ordered double-M elements, in which one transition metal occupies the perimeter layers and another fills the central M layers(for example, Mo_2TiC_2 and $Mo_2Ti_2C_3$, in which the outer M layers are Mo and the central M layers are Ti). Solid solutions on the X site produce carbonitrides. NA, not available.
Reprinted with permission from Ref. [29], Copyright 2017, Nature Publishing Group.

3 Advantages of 2D Nanomaterials

Compared with their bulk materials, 2D nanosheets exhibit unique properties in optics, electronics, mechanics, magnetism, and so on. Generally, there are some advances that have now been identified or uncovered for ultrathin 2D nanomaterials for energy storage and conversion, such as SCs, ORR, and HER. Firstly, the rich functionalization can be achieved on the in-plane and/or edge of 2D materials by heteroatoms doping, depositing with other active materials, and so on. Secondly, the larger specific area allows more atoms and active sites to interact with electrolyte ions to absorb and store ion, fasten surface redox reaction, and effectively reduce ion transport distance. Thirdly, better conductivity facilities electron transfer on the 2D surface. The bandgap also can be altered by doping and functionalization. Finally, the atomic thickness makes 2D materials more flexible and transparent for nanodevices. The thickness and transparency of these freestanding films *via* vacuum filtration, spin coating, drop casting, spray-coating, and inkjet printing can be controlled by the lateral size, concentration, solvents and so on.

4 Applications of 2D Nanomaterials

4.1 2D Nanomaterials for SCs

SCs are a new type of energy storage devices[93—96]. Different from batteries, they possess a large power density, long cycle life, and high reliability[97]. So far, in various markets of consumer electronics and transportation, SCs have been utilized to replace or combine with batteries[98]. Electrical double layer capacitor(EDLC) is a classical type of capacitors. Its specific capacitance is proportional to the available interfacial area where charges are stored by the formation of electrical double layer. Carbon materials like active carbon, porous carbon, carbon nanotubes, and graphene are typical electrical double layer capacitive materials[99—102]. At the surface of carbon materials, only reversible ion adsorption/desorption occurs without phase transformation[103]. Different from electric double-layer capacitor(EDLC), pseudocapacitors can store charges through a reversible redox reaction or intercalation on or near the surface of active materials without phase transition. Therefore, their specific capacitances are much larger[104]. Transition metal oxides(like RuO_2 and MnO_2), TMDs(like MoS_2), conducting polymers[like polythiophene(PT), polypyrrole(PPy) and polyaniline(PANI)], MXenes, and carbon materials with doped heteroatoms or surface functional groups[105—112] are typical pseudocapacitive materials. Among them, the pseudocapacitance of nanostructured TiO_2, Nb_2O_5, MoO_3, and MXenes in organic electrolytes are mainly attributed to the reversible ion intercalation by analyzing the cyclic voltammetry data at various sweep rates. Since no phase transition occurs in these materials and most charge storage sites are

located on the surface or near-surface region, the capacitive behavior is not diffusion-controlled but surface-dominated at a given rate, other than the battery-like behavior in battery-type electrodes, where intercalation happens in the bulk accompanied by phase change[113].

Most of pseudocapacitive materials can achieve a much higher capacity theoretically; however, the poor conductivity of some pseudocapacitive materials, such as metal oxides limits the rapid ion diffusion and electron transfer in a long region especially at high rate because there is not sufficient time to trigger ion diffusion into the interior structure[103,114]. Therefore, preparing corresponding ultrathin 2D nanosheets is an important way to improve the capacitance of these materials, because these ultrathin 2D nanomaterials always have larger specific area, rich active sites, and a better conductivity for beneficially utilizing their capacitive properties.

4.1.1 Graphene and Functionalized Graphene for SCs

The large specific area of graphene leads to a large specific capacitance. Theoretically, electrochemical double layer capacitance of monolayered graphene is 21 μF/cm^2, which means the specific capacitance of graphene can reach 550 F/g[115]. However, the lower actual specific area than theoretical values caused by defect, fold, and restacking makes it difficult to approach the theoretical specific capacitance. Moreover, the energy density based on pristine graphene is generally low as EDLC just happens at the partial accessible surface. For instance, a laminated four-layer graphene film exhibited an area capacitance of only 4.27 μF/cm^2[116].

Introducing ordered and/or disordered pores into the in-plane of graphene is a useful way to increase the available surface area. A much larger specific area can be achieved in etched porous graphene, resulting in a specific capacitance of 160 F/g[117]. Another way to enhance the capacitance of undoped graphene is to construct a 3D hierarchical structure. These macroporous or/and mesoporous networks facilitate efficient transfer of electrolyte around graphene. As an example, the CVD synthesized mesoporous graphene nanofibers(Fig.5) with an ultra large specific surface area of 2411 m^2/g exhibited a wide potential window up to 4 V and a high capacity of 193 F/g at 0.5 A/g with a retention of nearly 100% after 5000 cycles tested in ionic electrolytes[118].

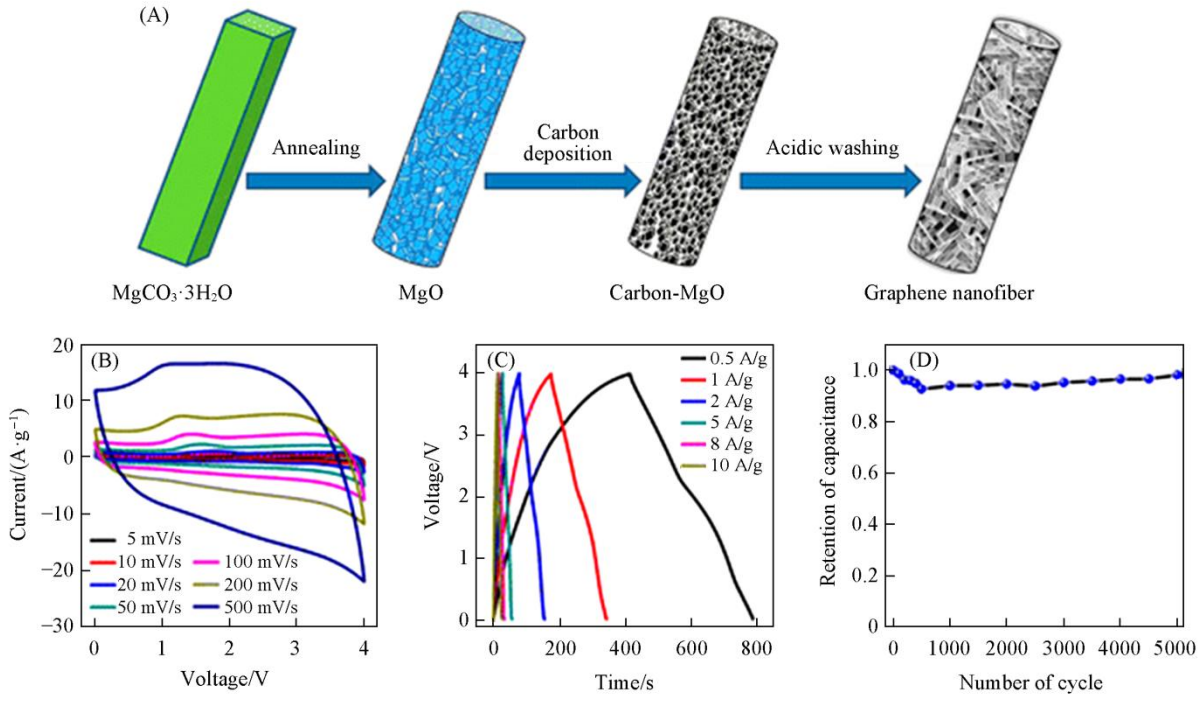

Fig.5 Growth mode of GNFs(A) , CV curves of GNFs as electrode in 4 V SCs(two-electrode coin cell) using $EMIBF_4$ as electrolyte(B), galvanostatic charge-discharge(GCD) curve(C) and retention of the relative capacitance of GNFs based SCs for 5000 cycle tests(D)

Reprinted with permission from Ref.[118], Copyright 2014, American Chemical Society.

Compared with pristine graphene, functionalized graphene by heteroatom doping and surface-group modification demonstrates a larger pseudocapacitance. For example, a nitrogen-superdoped 3D graphene network structure(3D GF-NG)(Fig.6) with a nitrogen-doping level up to 15.8% showed a remarkably excellent electrochemical behavior with a high specific capacitance of up to 380, 332, and 245 F/g in alkaline, acidic, and neutral electrolytes[119]. It was demonstrated that when nitrogen-doping level becomes higher, the supercapacitive performance is better. In other cases, lower nitrogen-doping level might be more beneficial for the enhanced capacitance since the nitrogen-doping with a higher level will break the conjugation of graphene plane. For example, 4.9% nitrogen-doped graphene *via* hydrothermally treating and then annealing GO/pyrrole at 1050 °C by Qu and co-workers[120] presented a specific capacitance of 484 F/g at 1 A/g. Oxygen-contained functionalized graphene *via* $Mg(OH)_2$ template-assisted low temperature reduction delivered both ultra-high specific

gravimetric and volumetric capacitances of 456 F/g and 470 F/cm^3[121]. In general, co-doping is better than single-doping for enhancing the capacitance. DFT calculation showed that fluorine can induce charge redistribution of nitrogen in carbon systems and reduce the gap between the highest occupied molecular orbital(HOMO) and the lowest unoccupied molecular orbital(LUMO) levels, decreasing the charge transfer resistance. A nitrogen, sulfur co-doped graphene hydrogel showed an excellent electrochemical performance with a specific capacitance as high as 566 F/g[122].

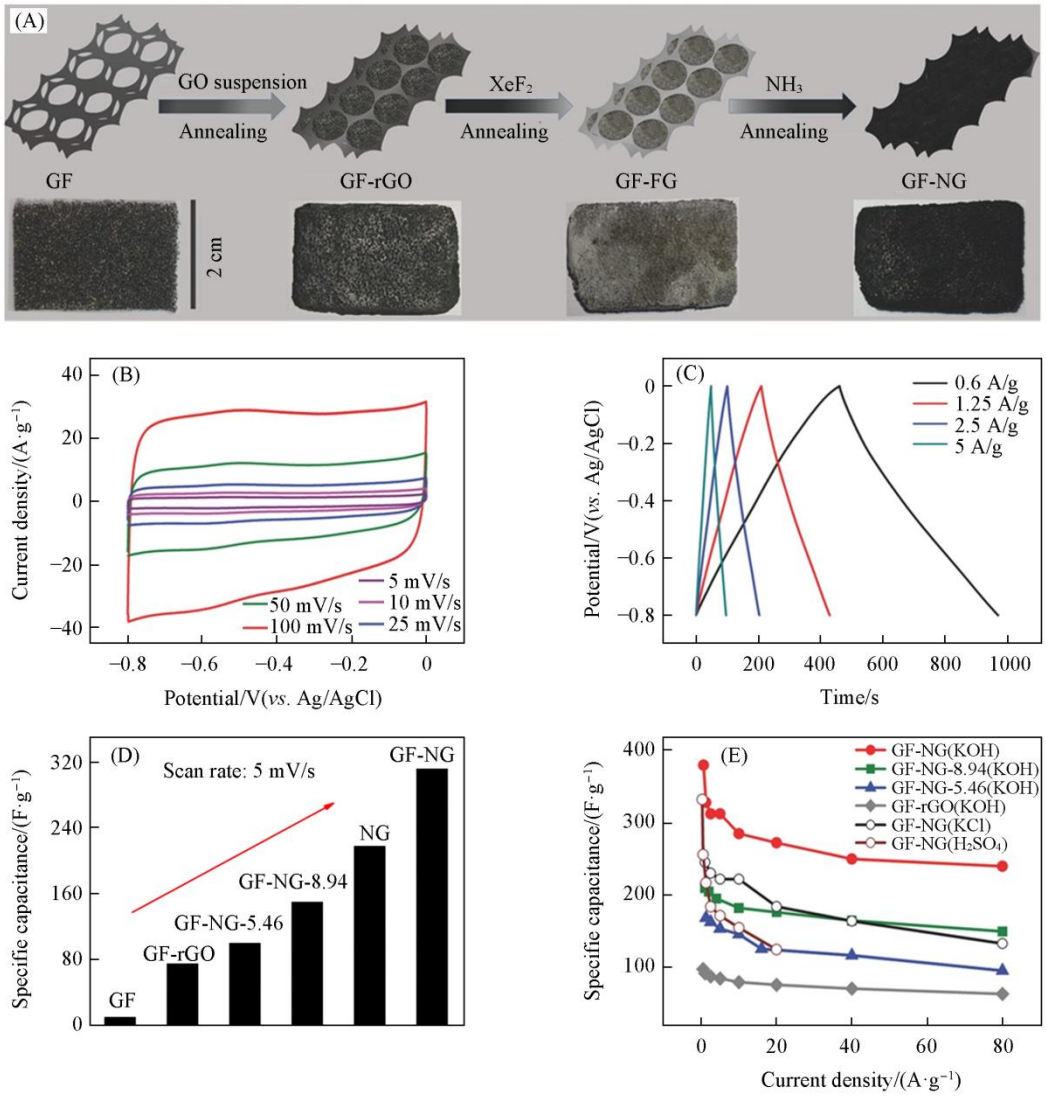

Fig.6 Schematic of the procedure for fabricating N-superdoped 3D graphene network structure(3D GF-NG) network macrostructure

(A) Electrochemical performances of GF-NG measured in three-electrode configuration; (B) CV curves at scan rates from 5 mV/s to 100 mV/s measured in 6.0 mol/L KOH for GF-NG; (C) GCD curves under different constant currents in 6.0 mol/L KOH for GF-NG; (D) the specific capacitance of GF, GF-rGO, GF-NGs and NG powder calculated by the CV curves at 5 mV/s; (E) the specific capacitance of GF-rGO and GF-NGs calculated at various current densities in 6.0 mol/L KOH, 1.0 mol/L KCl, and 1.0 mol/L H_2SO_4.
Reprinted with permission from Ref.[119], Copyright 2017, Wiley-VCH.

4.1.2 MXenes for SCs

Different from graphene and doped graphene, MXenes store charge *via* reversible intercalation of various cations (Na^+, K^+, NH_4^+, Mg^{2+}, and Al^{3+}) between $M_{n+1}X_nT_x$ layers[123]. Their high conductivities enable fast electron transfer in SCs. Gogotsi *et al.*[87] first prepared binder-free $Ti_3C_2T_x$ paper, which was highly flexible and yielded a volumetric capacitance of up to 350 F/cm^3 without degradation after 10000 cycles in basic solution. In H_2SO_4, the rolled films of $Ti_3C_2T_x$ achieved an extraordinary volumetric capacitance up to 900 F/cm^3 or 245 F/g[4,124]. Moreover, the surface atoms influence the electrochemical performance of MXene. Fluorine-terminated $Ti_3C_2T_x$ displayed a higher capacitance of 520 F/cm^3 in H_2SO_4 than the one with oxygenic functional groups[125]. The performance of MXene is also influenced by doping. DFT calculation indicated nitrogen-doping could increase the electron concentration, enhancing the electrical conductivity of MXene[126]. For instance, 15.48% nitrogen-doped Ti_2CT_x(Fig.7) presented an enhanced capacitance *via* carbonizing polymeric carbon nitride and Ti_2CT_x[127]. The content of doped nitrogen is also controlled simply by tuning the annealing temperature in ammonia[126].

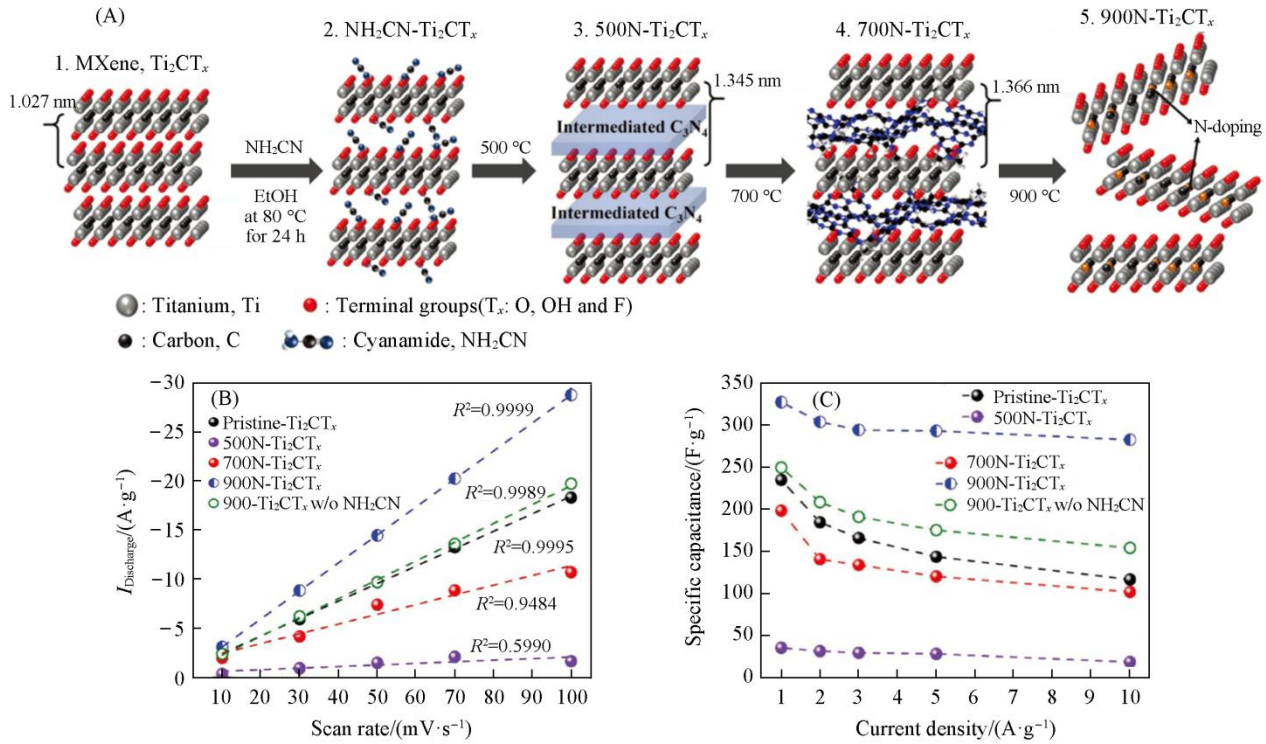

Fig.7 Schematic illustration of the synthesis procedures of p-C_3N_4 involved nitrogen doping in 2D Ti_2CT_x nanosheets(A), electrochemical characteristics of all pristine-Ti_2CT_x, 500N-Ti_2CT_x, 700N-Ti_2CT_x, 900N-Ti_2CT_x, and 900-Ti_2CT_x without NH_2CN electrodes with 6 mol/L KOH as the electrolyte with discharge current densities as a function of scan rate(B), gravimetric specific capacitance of all electrodes at various current densities, with 900N-Ti_2CT_x showing the highest capacitance(C)

Reprinted with permission from Ref.[127], Copyright 2018, Wiley-VCH.

4.2 2D Nanomaterials for ORR

ORR is at the heart of many fuel cell devices and holds a special place in the field of electrocatalysis. Generally, ORR involves either four-proton-electron pathway to reduce oxygen to water, which is desirable for fuel cells and metal-air batteries, or a two-proton-electron pathway to produce hydrogen peroxide. The pathway of ORR is determined by adsorption energetics of these intermediates and the reaction barriers on the surface of catalysts[128]. Noble metal(like platinum)-based catalysts can exhibit excellent ORR activity with a four proton-electron pathway, but the high cost and poor durability preclude their wide application[129]. Therefore, developing efficient, low-cost and durable non-noble metal electrocatalysts for the sluggish ORR is a key issue for practical applications.

4.2.1 Graphene and Doped Graphene for ORR

Pristine graphene is inert for electrocatalytic applications because there is no free electron for reaction. In contrast, in heteroatom and functional group doped graphene, effective intramolecular charge transfer leads to enhanced electrocatalytic activity. Nitrogen-doped graphene is the earliest investigated case, which exhibits not only an excellent $4e^-$ pathway for ORR, but also better tolerance towards methanol and CO than commercial Pt/C[130]. Pyridinic nitrogen, pyrrolic nitrogen, and graphitic nitrogen in nitrogen-doped graphene all contribute to the ORR activity. It remains controversial to determine which type of doping nitrogen is critical. Besides improving the intrinsic activity, constructing hierarchal porous structures is also effective to improve the ORR performance. For instance, a nanoporous 3D nitrogen-doped graphene material grown on nanoporous nickel *via* chemical vapor deposition(CVD) showed an outstanding catalytic activity towards ORR with a low onset potential of −0.08 V and a high kinetic current density of 8.2 mA/cm^2 at −0.4 V(*vs*. Ag/AgCl, measured in O_2-saturated 0.1 mol/L KOH)[131]. Sulfur-doped graphene by directly annealing GO and benzyl disulfide in argon at 1050 °C also exhibited a better ORR performance than undoped graphene[132]. As for phosphorous doping, DFT calculation implies that the ORR on phosphorous doped graphene proceeds by the combination of $2e^-$ and $4e^-$ pathways[133]. Although boron-doped graphene also exhibited an improved ORR activity over pristine graphene, the average electron transfer number n is only 3.5 at the potential window of fuel cell operation[134]. Dual-doped graphene usually reveals a higher activity toward ORR than single-doped graphene. Some researches demonstrated a homogeneous distribution of B and N with N—C and B—C bonding instead of B—N—C bonding can be formed in boron and nitrogen co-doped graphene[135]. Although the simulations show that the phosphorous atom is too large to be doped on the graphitic surface of carbon catalysts, and can only be effectively populated at edge sites, phosphorous site might stabilize the graphitic N and activate a neighboring C; this

enables the phosphorus and nitrogen co-doped graphene frameworks(PNGF, Fig.8) *via* a one-pot hydrothermal reaction with an ORR potential of 0.845 V *vs*. RHE at 3 mA/cm^2[136].

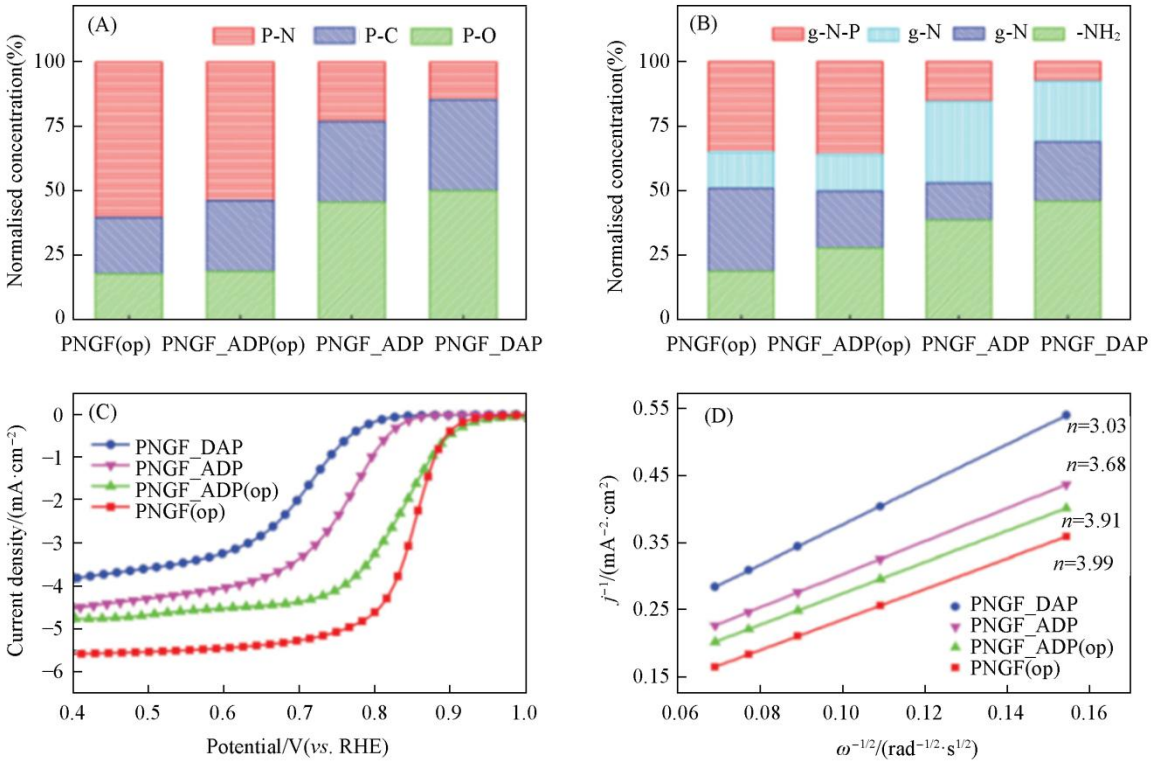

Fig.8 Relative ratio of XPS

P_{2p}(A) and N_{1s} binding configurations(B) for PNGF_DAP, PNGF_ADP, PNGF_ADP(op) and PNGF(op); (C) ORR activities of PNGF_DAP, PNGF_ADP, PNGF_ADP(op), and PNGF(op), measured by rotating disk electrode at 1600 r/min; (D) Koutecky-Levich plots of PNGF_DAP, PNGF_ADP, PNGF_ADP(op) and PNGF(op) at 0.6 V *vs*. RHE, derived from the corresponding linear sweep voltammograms.

Reprinted with permission from Ref.[136], Copyright 2017, Royal Society of Chemistry.

4.2.2 *Doped Graphdiyne for ORR*

Even though positive charges exist on *sp*-C in graphdiyne, they are not large enough to enhance OOH adsorption to facilitate ORR[137,138]. However, the original in-plane molecular pores of graphdiyne benefit the diffusion of O_2 and reactants[139]. After doping with heteroatoms *via* annealing pristine graphdiyne with heteroatom-contained sources, such as melamine, B_2O_3 or NH_3 at high temperature, doped graphdiyne shows a much-enhanced ORR activity[140—142]. For example, few-layer *sp*-N doped graphdiyne, which was prepared by introducing *sp*-N through pericyclic replacement of the acetylene groups and annealing with melamine, exhibits good ORR performance with a half-wave potential of 0.87 V in alkaline solution and a methanol resistance in acid solution (Fig.9)[143]. This is resulted from the better effect of *sp*-N than sp^2-N doping towards ORR[144]. Moreover, hydrogen atoms in hydrogen-substituted graphdiyne(HsGDY) are considered as edges or defects, which can be selectively doped by pyridinic N so that NHsGDY-900 °C exhibits a half-wave potential of 0.85 V and a limited current density of 6.2 mA/cm^2 in alkaline media due to the selectively high concentration of pyridinic N[145]. When two types of heteroatoms are doped simultaneously, N, F co-doped graphdiyne(NFGD) shows a higher ORR activity and stability than the N, B and N, S co-doped ones(NBGD and NSGD)[146].

4.2.3 *TMDs for ORR*

The catalytic performance of pure MoS_2 nanosheets is not ideal, but the presence of the uncoordinated metallic edge centers provides the chance of effective functionalization with various heteroatoms and groups. Functionalization effectively decreases the energy gap and improves the intrinsic conductivity of MoS_2 nanosheets, beneficial to the fast electron transport for ORR catalysis. Yu *et al.*[147] systematically explored the ORR performance of various doped MoS_2 by DFT calculation and found only the phosphorus doped MoS_2 has an oxygen adsorption energy close to that of Pt(111) surface. Experimentally, Song and co-workers[148] demonstrated that the doping of low-electronegative phosphorus atoms generated an extra ORR activity with four-electron selectivity, manifesting 7-folds current increase as well as 160 mV positive shift in both onset and half-wave potentials. They also synthesized oxygen-doped MoS_2(Fig.10), which showed a much-enhanced ORR activity over the pristine MoS_2 nanosheets[149]. However, the theoretical result indicated the P—Mo bridge site restricted the diffusion of hydrogen atom, limiting the ORR activity of phosphorus doped-MoS_2 nanosheet[150]. This limitation might be reduced by co-doping to enhance the binding strength between hydrogen and neighbor site sulfur[147,150]. The ORR activity of chemically exfoliated $MoSe_2$, WS_2, and WSe_2 exhibited no significant enhancements with increased surface areas after

exfoliation[151,152].

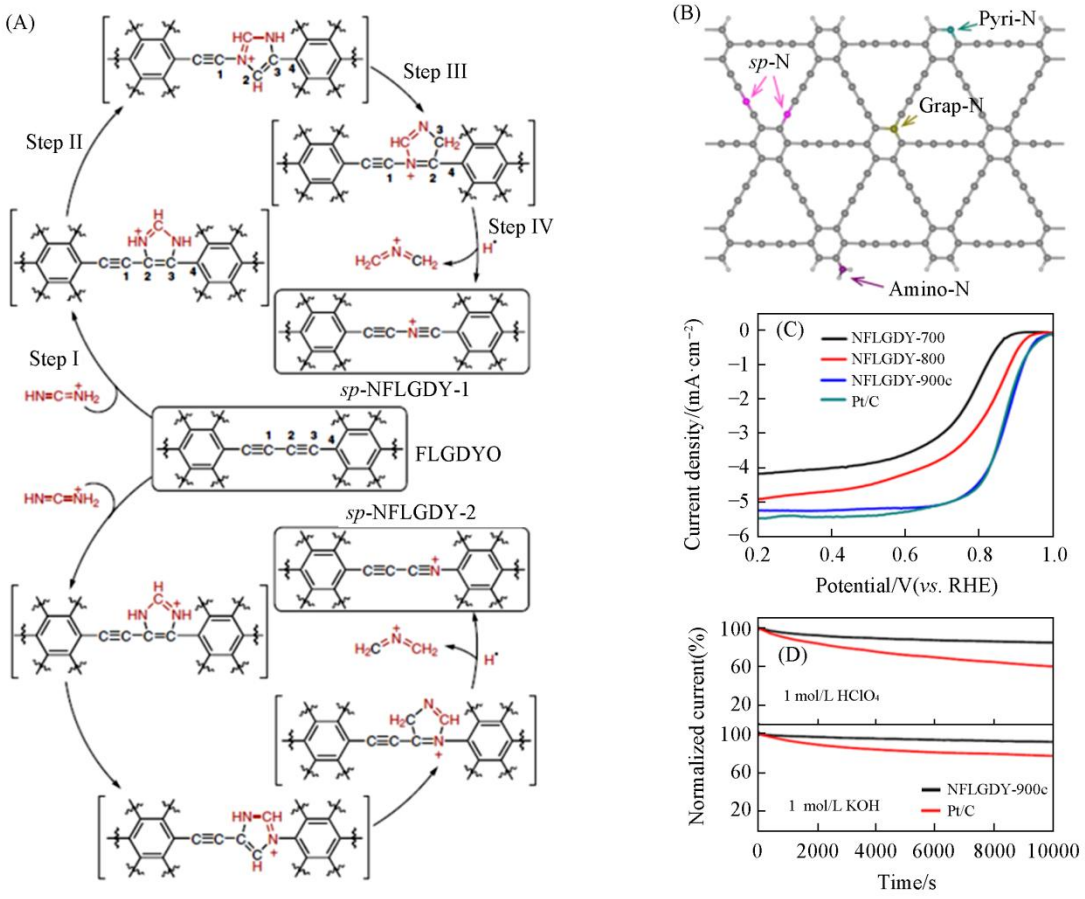

Fig.9 Synthesis of *sp*-N-doped few-layer GDY(A), geometries of N atoms in NFLGDY(the nitrogen doping forms include *sp*-N, pyri-N, amino-N and grap-N atoms)(B), ORR polarization curves of NFLGDY-700, NFLGDY-800, NFLGDY-900c and Pt/C catalysts at 1600 r/min in O_2-saturated 0.1 mol/L KOH(C) and *J-t* chronoamperometric responses of NFLGDY-900c and Pt/C in 0.1 mol/L $HClO_4$ and 0.1 mol/L KOH with NFLGDY-900c exhibiting greater stability(D)

Reprinted with permission from Ref.[143], Copyright 2018, Nature Publishing Group.

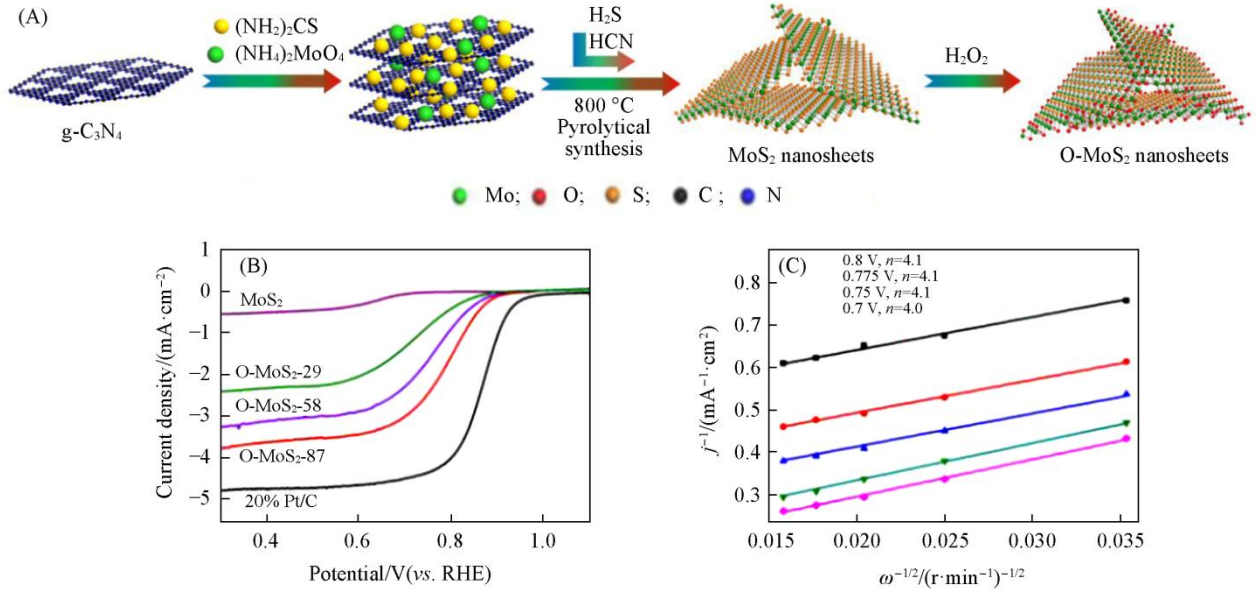

Fig.10 Proposed synthetic protocol for incorporated oxygen in MoS_2 ultrathin nanosheets(A), rotating disk electrode (RDE) current responses for O-MoS_2 and pristine MoS_2 nanosheets as well as 20% Pt/C at 2400 r/min and 10 mV/s in oxygen-saturated 0.1 mol/L KOH(B) and Koutecky-Levich plots for ORR catalysis at O-MoS_2(C)

Reprinted with permission from Ref.[149], Copyright 2015, Royal Society of Chemistry.

4.3 2D Nanomaterials for HER

HER is a classic example of a two-electron transfer reaction with one catalytic intermediate. The adsorbed hydrogen(H*) is formed *via* Volmer step then combined to produce hydrogen *via* either Heyrovsky or Tafel step[153]. The rate of the overall reaction largely depends on the hydrogen adsorption free energy (ΔG_{H^*}) and a value closed to zero is necessary for an active HER catalyst(Fig.11). This means the hydrogen binds to the surface of catalysts neither too strongly($\Delta G_{H^*}<0$) nor too weakly($\Delta G_{H^*}>0$)[154]. Besides ΔG_{H^*}, additional factor like morphology, size and pores of catalysts and pH will affect the kinetic barriers[155].

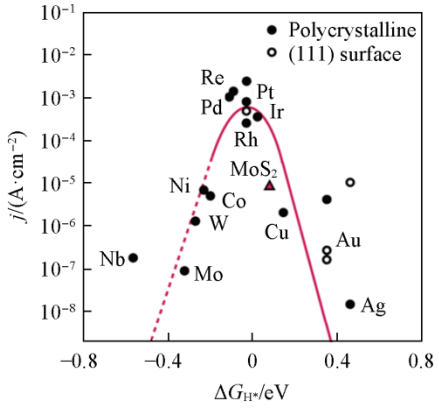

Fig.11 HER volcano plot for metals and MoS_2

Reprinted with permission from Ref.[128], Copyright 2017, AAAS.

4.3.1 *Graphene and Doped Graphene for HER*

The basal plane of pure graphene is considered to be inert for the HER with a relatively large(positive) ΔG_{H^*}(1.85 eV)[156]. Qiao and co-workers[157] found that among various single heteroatom doped graphene materials, boron-graphene showed the best specific HER activity(Fig.12). Their results also indicated nitrogen, sulfur co-doped graphene *via* annealing GO and dopant has a best HER activity with an overpotential of *ca.* 300 mV at 10 mA/cm^2 than single doped graphene, nitrogen, boron co-doped graphene and nitrogen, phosphorus co-doped graphene. By DFT, the most active dual-doped graphene model is nitrogen, sulfur co-doped graphene, represented by a lowest ΔG_{H^*} value of 0.23 eV. A nitrogen, sulfur co-doped nanoporous graphene synthesized by nanoporous nickel-based CVD even achieved an overpotential of 280 mV at 10 mA/cm^2 with a Tafel slope of 80.5 mV/dec by Chen *et al.*[158]. They found one carbon defect near sulfur doping site in the vicinity of graphitic nitrogen has the smallest ΔG_{H^*} value of 0.12 eV, which is comparable to platinum catalyst($\Delta G^{Pt}_{H^*} \approx 0.09$ eV).

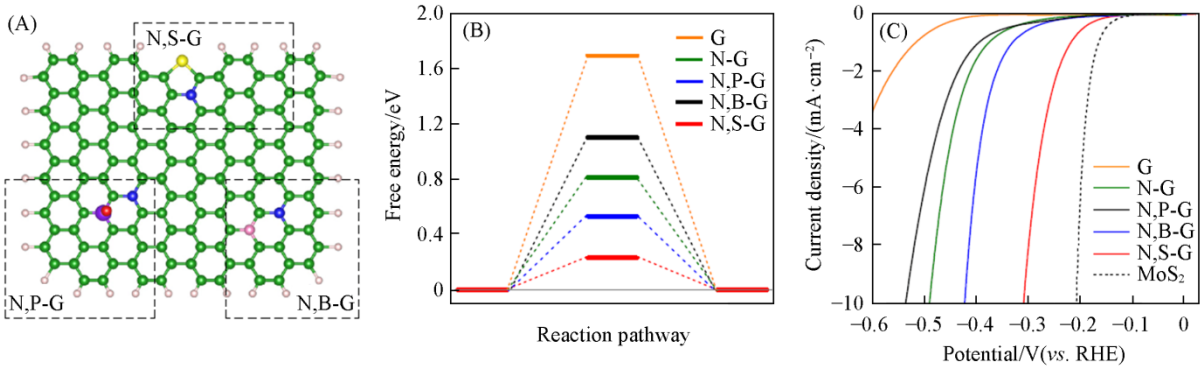

Fig.12 Atomic configurations of three dual-doped models with the lowest computed $|\Delta G_{H^*}|$(green, pink, blue, red, gold, purple and white represent carbon, boron, nitrogen, oxygen, sulfur, phosphorous and hydrogen atoms, respectively)(A), the three-state free energy diagram for the pure, single- and dual-doped graphene models(B) and polarization curves of various graphene-based materials in 0.5 mol/L H_2SO_4 with the benchmark MoS_2 under the same conditions for direct comparison(C)

Reprinted with permission from Ref.[157], Copyright 2016, Nature Publishing Group.

4.3.2 *TMDs for HER*

The bulk form of TMDs is not very efficient for HER, while the monolayered and nanostructured TMDs have been proved to possess higher concentration of catalytically active edges. Theoretically, TMDs are considered as the most ideal candidate to replace platinum for HER owing to their zero-approach Gibbs free energy of hydrogen adsorption[159]. As demonstrated by experimental and computational studies, the electrocatalytic HER activity of TMDs is mainly attributed to the edge of TMDs. It is also indicated that $MoSe_2$ is the best-performing catalyst($MoSe_2>WS_2>MoS_2>WSe_2$)[160]. Among those, MoS_2 is the first and the most studied TMD. The edges rather than the basal plane are proved catalytical activity for semiconducting 2H MoS_2. Compared to 2H phase, 1T and 1T′ MoS_2 is metallic and more conductive. Their metal edges exhibit a smaller near-zero ΔG_{H^*} value than 2H MoS_2. Moreover, some researchers predict the basal plane besides the edges of 1T and 1T′ MoS_2 has an HER activity[161]. Chhowalla *et al.*[162] proved that the activity of 2H MoS_2 was significantly reduced after oxidation, while 1T MoS_2 remained unaffected after oxidation. This is consistent with the prediction. By a three-step lithiation process using lithium-liquid ammonia medium, the mesoporous 1T MoS_2 even achieved an overpotential of 143 mV with a Tafel slope of only 43 mV/dec[163]. However, preparing a high phase-purity 1T and 1T′ MoS_2 remains a big challenge *via* lithium intercalation due to easily conversion to the stable 2H phase. Zhang and co-workers[164] synthesized 1T′-MoS_2 monolayers *via* multi-step annealing K_2MoO_4 and sulfur powder(Fig.13). They demonstrated that

the basal plane of 1T′ MoS_2 is highly efficient for HER, with an onset overpotential of only 65 mV and a current density(j) of 607 mA/cm^2 at an overpotential(η) of 400 mV.

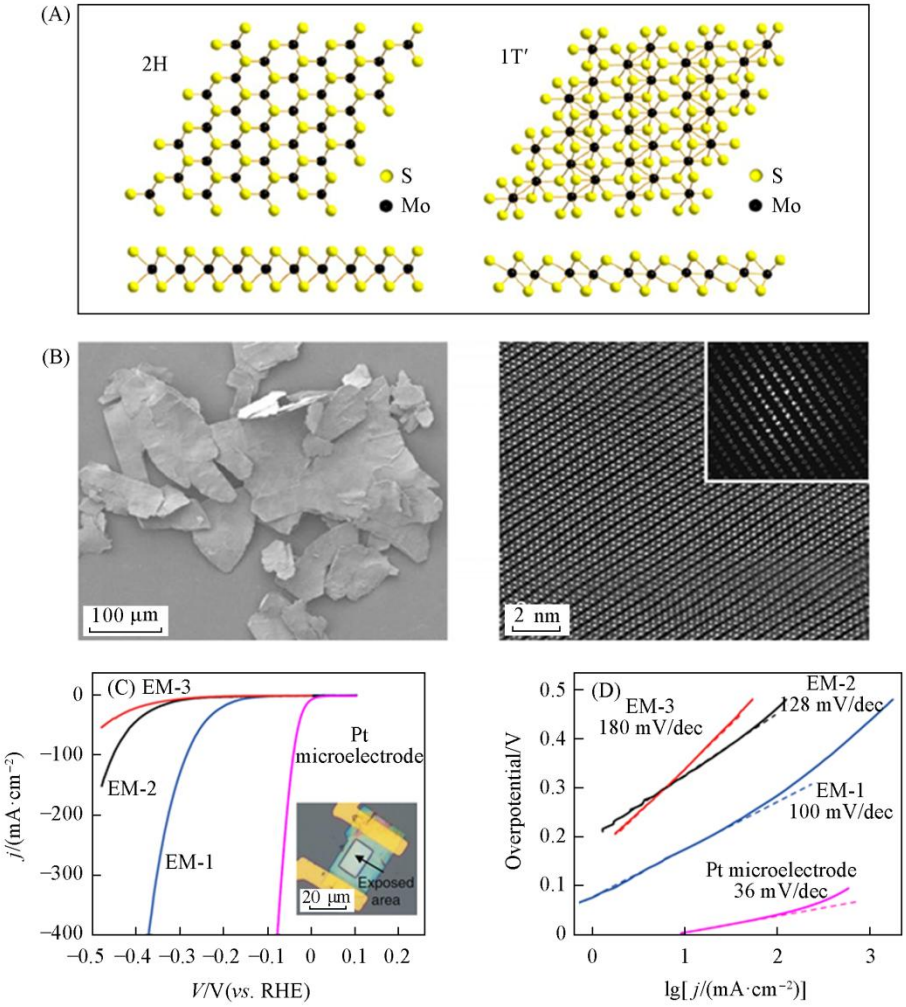

Fig.13 Schematic of 2H- and 1T′-MoS_2 structures(A), scanning electron microscopy(SEM) and scanning transmission electron microscopy(STEM) images of the prepared 1T′-MoS_2 crystals(B), polarization curves obtained with EM-1, EM-2 and EM-3(inset: optical microscope image of EM-1)(C) and Tafel plots obtained from the polarization curves in(C)(D)

Reprinted with permission from Ref.[164], Copyright 2018, Nature Publishing Group.

5 Summary and Outlook

2D materials provide both technological promise and new fundamental insight into important catalytic processes. Their unique properties make a good performance for energy storage and conversion. By tailoring their nanostructures, doping with heteroatoms and functional group, generating pores and phase transformation to modify the electronic and surface properties of graphene, TMDs, and MXenes, we are able to tune their electrocatalytic properties, allowing the development of high-performance SCs and highly selective, durable, and active catalysts for ORR and HER. Although research on 2D materials for energy storage and conversion rises only a few decades ago, great progress and many exciting achievements in preparation method, structural control and application have been made. Nevertheless, more efforts will be needed to understand the electrochemical behaviors of 2D materials in theory and by experiment. Firstly, more synthesis methods and relevant mechanisms should be explored for some 2D materials, such as graphdiyne. It is also meaningful to decrease the temperature or even develop more low-temperature methods in order to enable these 2D materials more green and cleaner. Secondly, it is inevitable to complicate the structure of 2D materials by doping even though an increased electrochemical performance is always achieved. In other to determine the real active sites and understand the electrochemical mechanism, more precise measurements at molecular level, stronger combination between the chemical structure and simulated model, and well-defined pure 2D materials are necessary to optimize their electrochemical behaviors. In this regard, 2D COFs, MOFs, graphdiyne and other polymers might be ideal modeling electrocatalysts, whose structures can be predesigned and detected by various technologies. However, it remains a big challenge of incorporating active sites into these 2D polymers to realize indispensable properties, such as high conductivity and tunable pore sizes for energy storage and conversion. Finally, other electrocatalytic reactions, such as CO_2 reduction and nitrogen reduction based

on 2D materials are highly promising for the sake of green carbon/nitrogen cycles and decreased fossil fuel carbon emissions. With the improvement of large-scale synthesis of 2D materials, in the future, the application of 2D materials for energy storage and conversion will provide new challenges and opportunities for researchers.

Acknowledgments

The authors thank the editors for kind invitation and AIST for financial supports. YANG Chao acknowledges financial support from Chinese Scholarship Council for his study in Japan and the support from S. M. in Japan Advanced Institute of Science and Technology.

References

[1] Novoselov K. S., Geim A. K., Morozov S. V., Jiang D., Zhang Y., Dubonos S. V., Grigorieva I. V., Firsov A. A., *Science*, **2004**, *306*, 666

[2] Sakamoto R., Fukui N., Maeda H., Matsuoka R., Toyoda R., Nishihara H., *Adv. Mater.*, **2019**, 1804211

[3] Chhowalla M., Shin H. S., Eda G., Li L. J., Loh K., Zhang H., *Nat. Chem.*, **2013**, *5*, 263

[4] Ghidiu M., Lukatskaya M. R., Zhao M. Q., Gogotsi Y., Barsoum M. W., *Nature*, **2014**, *516*, 78

[5] Lin Y., Williams T. V., Connell J. W., *J. Phys. Chem. Lett.*, **2010**, *1*, 277

[6] Zhang J., Chen Y., Wang X., *Energy Environ. Sci.,* **2015**, *8*, 3092

[7] Wang Q., O'Hare D., *Chem. Rev.*, **2012**, *112*, 4124

[8] Chen Y., Fan Z., Zhang Z., Niu W., Li C., Yang N., Chen B., Zhang H., *Chem. Rev.*, **2018**, *118*, 6409

[9] Peng Y., Li Y., Ban Y., Jin H., Jiao W., Liu X., Yang W., *Science*, **2014**, *346*, 1356

[10] Colson J. W., Woll A. R., Mukherjee A., Levendorf M. P., Spitler E. L., Shields V. B., Spencer M. G., Park J., Dichtel W. R., *Science*, **2011**, *332*, 228

[11] Kory M. J., Wörle M., Weber T., Payamyar P., van de Poll S. W., Dshemuchadse J., Trapp N., Schlüter A. D., *Nat. Chem.*, **2014**, *6*, 779

[12] Li L., Yu Y., Ye G. J., Ge Q., Ou X., Wu H., Feng D., Chen X. H., Zhang Y., *Nat. Nanotechnol.,* **2014**, *9*, 372

[13] Dou L., Wong A. B., Yu Y., Lai M., Kornienko N., Eaton S. W., Fu A., Bischak C. G., Ma J., Ding T., Ginsberg N. S., Wang L. W., Alivisatos A. P., Yang P., *Science*, **2015**, *349*, 1518

[14] Jin H., Guo C., Liu X., Liu J., Vasileff A., Jiao Y., Zheng Y., Qiao S. Z., *Chem. Rev.*, **2018**, *118*, 6337

[15] Sial M. A. Z. G., Din M. A. U., Wang X., *Chem. Soc. Rev.*, **2018**, *47*, 6175

[16] Wang X., Weng Q., Yang Y., Bando Y., Golberg D., *Chem. Soc. Rev.*, **2016**, *45*, 4042

[17] Wang X., Sun G., Lia N., Chen P., *Chem. Soc. Rev.*, **2016**, *45*, 2239

[18] Xue Y., Zhang Q., Wang W., Cao H., Yang Q., Fu L., *Adv. Energy Mater.*, **2017**, *7*, 1602684

[19] Tan C., Cao X., Wu X. J., He Q., Yang J., Zhang X., Chen J., Zhao W., Han S., Nam G. H., Sindoro M., Zhang H., *Chem. Rev.*, **2017**, *117*, 6225

[20] Kumar A., Xu Q., *Chem. Nano Mat.*, **2018**, *4*, 28

[21] Nicolosi V., Chhowalla M., Kanatzidis M. G., Strano M. S., Coleman J. N., *Science*, **2013**, *340*, 1226419

[22] Cai X., Luo Y., Liu B., Cheng H. M., *Chem. Soc. Rev.*, **2018**, *47*, 6224

[23] Zhang X., Xie Y., *Chem. Soc. Rev.*, **2013**, *42*, 8187

[24] Sun Y., Gao S., Xie Y., *Chem. Soc. Rev.*, **2014**, *43*, 530

[25] Novoselov K. S., Jiang D., Schedin F., Booth T. J., Khotkevich V. V., Morozov S. V., Geim A. K., Proc. *Natl. Acad. Sci.*, **2005**, *102*, 10451

[26] Coleman J. N., Lotya M., O'Neill A., Bergin S. D., King P. J., Khan U., Young K., Gaucher A., De S., Smith R. J., Shvets I. V., Arora S. K., Stanton G., Kim H. Y., Lee K., Kim G. T., Duesberg G. S., Hallam T., Boland J. J., Wang J. J., Donegan J. F., Grunlan J. C., Moriarty G., Shmeliov A., Nicholls R. J., Perkins J. M., Grieveson E. M., Theuwissen K., McComb D. W., Nellist P. D., Nicolosi V., *Science*, **2011**, *331*, 568

[27] Huang X., Zeng Z., Zhang H., *Chem. Soc. Rev.*, **2013**, *42*, 1934

[28] Dong L., Yang J., Chhowalla M., Loh K. P., *Chem. Soc. Rev.*, **2017**, *46*, 7306

[29] Anasori B., Lukatskaya M. R., Gogotsi Y., *Nat. Rev. Mater.*, **2017**, *2*, 16098.

[30] Dines M. B., *Mater. Res. Bull.*, **1975**, *10*, 287

[31] Hummers W., Offeman R., *J. Am. Chem. Soc.*, **1958**, *80*, 1339

[32] Paton K. R., Varrla E., Backes C., Smith R. J., Khan U., O'Neill A., Boland C., Lotya M., Istrate O. M., King P., Higgins T., Barwich S., May P., Puczkarski P., Ahmed I., Moebius M., Pettersson H., Long E., Coelho J., O'Brien S. E., McGuire E. K., Sanchez B. M., Duesberg G. S., McEvoy N., Pennycook T. J., Downing C., Crossley A., Nicolosi V., Coleman J. N., *Nat. Mater.*, **2014**, *13*, 624

[33] Matsumoto M., Saito Y., Park C., Fukushima T., Aida T., *Nat. Chem.*, **2015**, *7*, 730

[34] Hernandez Y., Nicolosi V., Lotya M., Blighe F. M., Sun Z. Y., De S., McGovern I. T., Holland B., Byrne M., Gun'ko Y. K., Boland J. J., Niraj P., Duesberg G., Krishnamurthy S., Goodhue R., Hutchison J., Scardaci V., Ferrari A. C., Coleman J. N., *Nat. Nanotechnol.*, **2008**, *3*, 563

[35] Yu J., Li J., Zhang W., Chang H., *Chem. Sci.*, **2015**, *6*, 6705

[36] Zhang Y., Zhang L., Zhou C., *Acc. Chem. Res.*, **2013**, *46*, 2329

[37] Ji Q., Zhang Y., Zhang Y., Liu Z., *Chem. Soc. Rev.*, **2015**, *44*, 2587

[38] Shi Y., Li H., Li L. J., *Chem. Soc. Rev.*, **2015**, *44*, 2744

[39] Du X., Skachko I., Barker A., Andrei E. Y., *Nat. Nanotechnol.*, **2008**, *3*, 491

[40] Dawlaty J. M., Shivaraman S., Chandrashekhar M., Rana F., Spencer M. G., *Appl. Phys. Lett.*, **2008**, *92*, 42116

[41] Balandin A. A., Ghosh S., Bao W., Calizo I., Teweldebrhan D., Miao F., Lau C. N., *Nano Lett.*, **2008**, *8*, 902

[42] Lee C., Wei X. D., Kysar J. W., Hone J., *Science*, **2008**, *321*, 385

[43] Novoselov K. S., *ECS Transactions*, **2009**, *19*, 3

[44] Li G., Li Y., Liu H., Guo Y., Li Y., Zhu D., *Chem. Commun.*, **2010**, *46*, 3256

[45] Dai L., Xue Y., Qu L., Choi H. J., Baek J. B., *Chem. Rev.*, **2015**, *115*, 4823

[46] Yang C., Dong L., Chen Z., Lu H., *J. Phys. Chem. C*, **2014**, *118*, 18884

[47] Navalon S., Dhakshinamoorthy A., Alvaro M., Antonietti M., García H., *Chem. Soc. Rev.*, **2017**, *46*, 4501

[48] Asefa T., *Acc. Chem. Res.*, **2016**, *49*, 1873

[49] Wu P., Du P., Zhang H., Cai C., *Phys. Chem. Chem. Phys.*, **2013**, *15*, 6920

[50] Rani P., Jindal V. K., *RSC Adv.*, **2013**, *3*, 802

[51] Kong X., Chen Q., Sun Z., *ChemPhysChem*, **2013**, *14*, 514

[52] Liang J., Jiao Y., Jaroniec M., Qiao S. Z., *Angew. Chem. Int. Ed.*,

2012, *51*, 11496
[53] Wang X., Sun G., Routh P., Kim D. H., Huang W., Chen P., *Chem. Soc. Rev.*, **2014**, *43*, 7067
[54] Karlicky F., Datta K. K. R., Otyepka M., Zboril R., *ACS Nano*, **2013**, *7*, 6434
[55] Jeon I. Y., Choi H. J., Choi M., Seo J. M., Jung S. M., Kim M. J., Zhang S., Zhang L., Xia Z., Dai L., Park N., Baek J. B., *Sci. Rep.*, **2013**, *3*, 1810
[56] Zhang J., Dai L., *Angew. Chem. Int. Ed.*, **2016**, *55*, 13296
[57] Georgakilas V., Otyepka M., Bourlinos A. B., Chandra V., Kim N., Kemp K. C., Hobza P., Zboril R., Kim K. S., *Chem. Rev.*, **2012**, *112*, 6156
[58] Chua C. K., Pumera M., *Chem. Soc. Rev.*, **2013**, *42*, 3222
[59] Quintana M., Spyrou K., Grzelczak M., Browne W. R., Rudolf P., Prato M., *ACS Nano*, **2010**, *4*, 3527
[60] Xu Y., Bai H., Lu G., Li C., Shi G. Q., *J. Am. Chem. Soc.*, **2008**, *130*, 5856
[61] Yan L., Zheng Y. B., Zhao F., Li S. J., Gao X. F., Xu B. Q., Weiss P. S., Zhao Y. L., *Chem. Soc. Rev.*, **2012**, *41*, 97
[62] Ambrosi A., Chua C. K., Latiff N. M., Loo A. H., Wong C. H. A., Eng A. Y. S., Bonanni A., Pumera M., *Chem. Soc. Rev.*, **2016**, *45*, 2458
[63] Gao X., Liu H., Wang D., Zhang J., *Chem. Soc. Rev.*, **2019**, *48*, 908
[64] Huang C., Li Y., Wang N., Xue Y., Zuo Z., Liu H., Li Y., *Chem. Rev.*, **2018**, *118*, 7744
[65] Kang B., Shi H., Wu S., Zhao W., Ai H., Lee J. Y., *Carbon*, **2017**, *123*, 415
[66] Shang H., Zuo Z., Zheng H., Li K., Tu Z., Yi Y., Liu H., Li Y., Li Y., *Nano Energy*, **2018**, *44*, 144
[67] Zhao J., Chen Z., Zhao J., *J. Mater. Chem. A*, **2019**, *7*, 4026
[68] Zhang J., Chen G., Müllen K., Feng X., *Adv. Mater.*, **2018**, *30*, 1800528
[69] Gu J., Magagula S., Zhao J., Chen Z., *Small Methods*, **2019**, 1800550
[70] Das B. K., Sen D., Chattopadhyay K. K., *Phys. Chem. Chem. Phys.*, **2016**, *18*, 2949
[71] He J., Wang N., Yang Z., Shen X., Wang K., Huang C., Yi Y., Tu Z., Li Y., *Energy Environ. Sci.*, **2018**, *11*, 2893
[72] Wang N., He J., Tu Z., Yang Z., Zhao F., Li X., Huang C., Wang K., Jiu T., Yi Y., Li Y., *Angew. Chem. Int. Ed.*, **2017**, *56*, 10740
[73] Farimani A. B., Min K., Aluru N. R., *ACS Nano*, **2014**, *8*, 7914
[74] Krasnozhon D., Lembke D., Nyffeler C., Leblebici Y., Kis A., *Nano Lett.*, **2014**, *14*, 5905
[75] Lv R., Robinson J. A., Schaak R. E., Sun D., Sun Y., Mallouk T. E., Terrones M., *Acc. Chem. Res.*, **2014**, *48*, 56
[76] Splendiani A., Sun L., Zhang Y. B., Li T. S., Kim J., Chim C. Y., Gali G., Wang F., *Nano Lett.*, **2010**, *10*, 1271
[77] Voiry D., Mohite A., Chhowalla M., *Chem. Soc. Rev.*, **2015**, *44*, 2702
[78] Acerce M., Voiry D., Chhowalla M., *Nat. Nanotechnol.*, **2015**, *10*, 313
[79] Li H., Jia X., Zhang Q., Wang X., *Chem.*, **2018**, *4*, 1
[80] Gutiérrez H. R., Perea-López N., Elía A. L., Berkdemir A., Wang B., Lv R., López-Urías F., Crespi V. H., Terrones H., Terrones M., *Nano Lett.*, **2013**, *13*, 3447
[81] Wang Z., Shen Y., Ito Y., Zhang Y., Du J., Fujita T., Hirata A., Tang Z., Chen M., *ACS Nano*, **2018**, *12*, 1571
[82] Eda G., Yamaguchi H., Voiry D., Fujita T., Chen M. W., Chhowalla M., *Nano Lett.*, **2011**, *11*, 5111
[83] Tang H., Wang J., Yin H., Zhao H., Wang D., Tang Z., *Adv. Mater.*, **2015**, *27*, 1117
[84] Chou S. S., Sai N., Lu P., Coker E. N., Liu S., Artyushkova K., Luk T. S., Kaehr B., Brinker C. J., *Nat. Commun.*, **2015**, *6*, 8311
[85] Lauritsen J. V., Kibsgaard J., Helveg S., Topsøe H., Clausen B. S., Lægsgaard E., Besenbacher F., *Nat. Nanotechnol.*, **2007**, *2*, 53
[86] Hu Z., Wu Z., Han C., He J., Ni Z., Chen W., *Chem. Soc. Rev.*, **2018**, *47*, 3100
[87] Naguib M., Kurtoglu M., Presser V., Lu J., Niu J., Heon M., Hultman L., Gogotsi Y., Barsoum M. W., *Adv. Mater.*, **2011**, *23*, 4248
[88] Chaudhari N. K., Jin H., Kim B., San Baek D., Joo S. H., Lee K., *J. Mater. Chem. A*, **2017**, *5*, 24564
[89] Xiong D., Li X., Bai Z., Lu S., *Small*, **2018**, *14*, 1703419
[90] Lukatskaya M. R., Mashtalir O., Ren C. E., Dall'Agnese Y., Rozier P., Taberna P. L., Naguib M., Simon P., Barsoum M. W., Gogotsi Y., *Science*, **2013**, *341*, 1502.
[91] Ng V. M. H., Huang H., Zhou K., Lee P. S., Que W., Xu J. Z., Kong L. B., *J. Mater. Chem. A*, **2017**, *5*, 3039
[92] Naguib M., Mochalin V. N., Barsoum M. W., Gogotsi Y., *Adv. Mater.*, **2014**, *26*, 992
[93] Chen K., Xue D., *Chem. Rec.*, **2018**, *18*, 282
[94] Chen K., Xue D., *Nanotechnology*, **2017**, *29*, 024003.
[95] Chen K., Xue D., *Scientia Sinica Technologica*, **2018**, *49*, 175
[96] Chen K., Xue D., *Funct. Mater. Lett.*, **2019**, *12*, 1830005
[97] Simon P., Gogotsi Y., *Nat. Mater.*, **2008**, *7*, 845
[98] Wang F., Wu X., Yuan X., Liu Z., Zhang Y., Fu L., Zhu Y., Zhou Q., Wu Y., Huang W., *Chem. Soc. Rev.*, **2017**, *46*, 6816
[99] Hu Y., Zhao Y., Li Y., Li H., Qu L., Xie X., Dai L. M., *Chem. Res. Chinese Universities*, **2012**, *28*(2), 302
[100] Pachfule P., Shinde D., Majumder M., Xu Q., *Nat. Chem.*, **2016**, *8*, 718
[101] Liang Z., Zhao R., Qiu T., Zou R., Xu Q., *Energy Chem.*, **2019**, *1*, 100001
[102] Liang X., Chen K., Xue D., *Adv. Energy Mater.*, **2018**, *8*, 1703329
[103] Yu X., Yun S., Yeon J. S., Bhattacharya P., Wang L., Woo L. S., Hu X., Park H. S., *Adv. Energy Mater.*, **2018**, *8*, 1702930
[104] Wang Y., Song Y., Xia Y., *Chem. Soc. Rev.*, **2016**, *45*, 5925
[105] Yang C., Chen Z., Shakir I., Xu Y., Lu H., *Nano Res.*, **2016**, *9*, 951
[106] Zhang Q. F., Uchaker E., Candelaria S. L., Cao G. Z., *Chem. Soc. Rev.*, **2013**, *42*, 3127
[107] Yu G., Xie X., Pan L., Bao Z., Cui Y., *Nano Energy*, **2013**, *2*, 213
[108] Hu C., Song L., Zhang Z., Chen N., Feng Z., Qu L., *Energy Environ. Sci.*, **2015**, *8*, 31
[109] Zhang C., Lv W., Tao Y., Yang Q. H., *Energy Environ. Sci.*, **2015**, *8*, 1390
[110] Wang H., Wu Y., Yuan X., Zeng G., Zhou J., Wang X., Chew J. W., *Adv. Mater.*, **2018**, *30*, 1704561
[111] Kong L. B., Zhang J., Cai J. J., Yang Z. S., Luo Y. C., Kang L., *Chem. Res. Chinese Universities*, **2011**, *27*(2), 295
[112] Wang H., Shi X., Shi Y., Zhang W., Yao S., *Chem. Res. Chinese Universities*, **2017**, *33*(4), 638
[113] Brezesinski T., Wang J., Tolbert S. H., Dunn B., *Nat. Mater.*, **2010**, *9*, 146
[114] Augustyn V., Come J., Lowe M. A., Kim J. W., Taberna P. L., Tolbert S. H., Abrua H. D., Simon P., Dunn B., *Nat. Mater.*, **2013**, *12*, 518
[115] Xia J., Chen F., Li J., Tao N., *Nat. Nanotechnol.*, **2009**, *4*, 505
[116] Xu P., Kang J., Choi J. B., Suhr J., Yu J., Li F., Byun J. H., Kim B. S., Chou T. W., *ACS Nano*, **2014**, *8*, 9437
[117] Zhu Y., Murali S., Stoller M. D., Ganesh K. J., Cai W., Ferreira P. J.,

Pirkle A., Wallace R. M., Cychosz K. A., Thommes M., Su D., Stach E. A., Ruoff R. S., *Science*, **2011**, *332*, 1537

[118] Cui C., Qian W., Yu Y., Kong C., Yu B., Xiang L., Wei F., *J. Am. Chem. Soc*., **2014**, *136*, 2256

[119] Zhang W., Xu C., Ma C., Li G., Wang Y., Zhang K., Li F., Liu C., Cheng H. M., Du Y., Tang N., Ren W., *Adv. Mater.*, **2017**, *29*, 1701677

[120] Zhao Y., Hu C., Hu Y., Cheng H., Shi G., Qu L., *Angew. Chem. Int. Ed.*, **2012**, *51*, 11371

[121] Yan J., Wang Q., Wei T., Jiang L., Zhang M., Jing X., Fan Z., *ACS Nano*, **2014**, *8*, 4720

[122] Wang T., Wang L. X., Wu D. L., Xia W., Jia D. Z., *Sci. Rep*., **2015**, *5*, 9591

[123] Okubo M., Sugahara A., Kajiyama S., Yamada A., *Acc. Chem. Res.*, **2018**, *51*, 591

[124] Salanne M., Rotenberg B., Naoi K., Kaneko K., Taberna P. L., Grey C. P., Dunn B., Simon P., *Nat. Energy*, **2016**, *1*, 16070

[125] Dall'Agnese Y., Lukatskaya M. R., Cook K. M., Taberna P. L., Gogotsi Y., Simon P., *Electrochem. Commun.*, **2014**, *48*, 118

[126] Wen Y., Rufford T. E., Chen X., Li N., Lyu M., Dai L., Wang L., *Nano Energy*, **2017**, *38*, 368

[127] Yoon Y., Lee M., Kim S. K., Bae G., Song W., Myung S., Lim J., Lee S. S., Zyung T., An K. S., *Adv. Energy Mater.*, **2018**, 1703173

[128] Seh Z. W., Kibsgaard J., Dickens C. F., Chorkendorff I. B., Nørskov J. K., Jaramillo T. F., *Science*, **2017**, *355*, eaad4998

[129] Borup R., Meyers J., Pivovar B., Kim Y. S., Mukundan R., Garland N., Myers D., Wilson M., Garzon F., Wood D., Zelenay P., More K., Stroh K., Zawodzinski T., Boncella J., McGrath J. E., Inaba M., Miyatake K., Hori M., Ota K., Ogumi Z., Miyata S., Nishikata A., Siroma Z., Uchimoto Y., Yasuda K., Kimijima K. I., Iwashita N., *Chem. Rev.*, **2007**, *107*, 3904

[130] Qu L., Liu Y., Baek J. B., Dai L., *ACS Nano*, **2010**, *4*, 1321

[131] Ito Y., Qiu H. J., Fujita T., Tanabe Y., Tanigaki K., Chen M., *Adv. Mater.*, **2014**, *26*, 4145

[132] Yang Z., Yao Z., Li G., Fang G., Nie H., Liu Z., Zhou X., Chen X., Huang S., *ACS Nano*, **2012**, *6*, 205

[133] Zhang X., Lu Z., Fu Z., Tang Y., Ma D., Yang Z., *J. Power Sources*, **2015**, *276*, 222

[134] Sheng Z. H., Gao H. L., Bao W. J., Wang F. B., Xia X. H., *J. Mater. Chem.*, **2012**, *22*, 390

[135] Wu J., Rodrigues M. T. F., Vajtai R., Ajayan P. M., *Adv. Mater.*, **2016**, *28*, 6239

[136] Chai G. L., Qiu K., Qiao M., Titirici M. M., Shang C., Guo Z., *Energy Environ. Sci.*, **2017**, *10*, 1186

[137] Kang B., Lee J. Y., *J. Phys. Chem. C,* **2014**, *118*, 12035

[138] Kang B., Wu S., Ma J., Ai H., Lee, J. Y., *Nanoscale*, **2019**, *11*, 16599

[139] Wang N., He J., Wang K., Zhao Y., Jiu T., Huang C., Li Y., *Adv. Mater.,* **2019**, 1803202

[140] Lv Q., Si W., Yang Z., Wang N., Tu Z., Yi Y., Huang C., Jiang L., Zhang M., He J., Long Y., *ACS Appl. Mater. Interfaces*, **2017**, *9*, 29744

[141] Zhao Y., Tang H., Yang N., Wang D., *Adv. Sci.*, **2018**, *5*, 1800959

[142] Yu H., Xue Y., Li Y., *Adv. Mater.*, **2019**, 1803101

[143] Zhao Y., Wan J., Yao H., Zhang L., Lin K., Wang L., Yang N., Liu D., Song L., Zhu J., Gu L., Liu L., Zhao H., Li Y., Wang D., *Nat. Chem.*, **2018**, *10*, 924

[144] Feng Z., Ma Y., Li Y., Li R., Liu J., Li H., Tang Y., Dai X., *J. Phys.: Condens. Matter*, **2019**, *31*, 465201

[145] Lv Q., Si W., He J., Sun L., Zhang C., Wang N.,Yang Z., Li X., Wang X., Deng W., Long Y., Huang C., Li Y., *Nat. Commun.*, **2018**, *9*, 3376

[146] Zhang S., Cai Y., He H., Zhang Y., Liu R., Cao H., Wang M., Liu J., Zhang G., Li Y., Liu H., Li B., *J. Mater. Chem. A*, **2016**, *4*, 4738

[147] Zhang X., Shi S., Gu T., Li L., Yu S., *Phys. Chem. Chem. Phys.*, **2018**, *20*, 18184

[148] Huang H., Feng X., Du C., Song W., *Chem. Commun.*, **2015**, *51*, 7903

[149] Huang H., Feng X., Du C., Song W., *J. Mater. Chem. A*, **2015**, *3*, 16050

[150] Zhang H., Tian Y., Zhao J., Cai Q., Chen Z., *Electrochim. Acta*, **2017**, *225*, 543

[151] Chua X. J., Luxa J., Eng A. Y. S., Tan S. M., Sofer Z., Pumera M., *ACS Catal.*, **2016**, *6*, 5724

[152] Eng A. Y. S., Ambrosi A., Sofer Z., Simek P., Pumera M., *ACS Nano*, **2014**, *8*, 12185

[153] Jiao Y., Zheng Y., Jaroniec M., Qiao S. Z., *Chem. Soc. Rev.*, **2015**, *44*, 2060

[154] Nørskov J. K., Bligaard T., Logadottir A., Kitchin J. R., Chen J. G., Pandelov S., Stimming U., *J. Electrochem. Soc.*, **2005**, *152*, J23

[155] Strmcnik D., Uchimura M., Wang C., Subbaraman R., Danilovic N., van der Vliet D., Paulikas A. P., Stamenkovic V. R., Markovic N. M., *Nat. Chem.*, **2013**, *5*, 300

[156] Zheng Y., Jiao Y., Li L. H., Xing T., Chen Y., Jaroniec M., Qiao S. Z., *ACS Nano*, **2014**, *8*, 5290

[157] Jiao Y., Zheng Y., Davey K., Qiao S. Z., *Nat. Energy*, **2016**, *1*, 16130

[158] Ito Y., Cong W., Fujita T., Tang Z., Chen M., *Angew. Chem. Int. Ed.*, **2014**, *54*, 2131

[159] Hinnemann B., Moses P. G., Bonde J., Jørgensen K. P., Nielsen J. H., Horch S., Chorkendorff I., Nørskov J. K., *J. Am. Chem. Soc.*, **2005**, *127*, 5308

[160] Tsai C., Chan K., Abild-Pedersen F., Norskov J. K., *Phys. Chem. Chem. Phys.*, **2014**, *16*, 13156

[161] Fan X. L., Yang Y., Xiao P., Lau W. M., *J. Mater. Chem. A*, **2014**, *2*, 20545

[162] Voiry D., Salehi M., Silva R., Fujita T., Chen M., Asefa T., Shenoy V. B., Eda G., Chhowalla M., *Nano Lett.*, **2013**, *13*, 6222

[163] Yin Y., Han J., Zhang Y., Zhang X., Xu P., Yuan Q., Samad L., Wang X., Wang Y., Zhang Z., Zhang P., Cao X., Song B., Jin S., *J. Am. Chem. Soc.*, **2016**, *138*, 7965

[164] Yu Y. F., Nam G. H., Wu X. J., Zhang K., Yang Z. Z., Chen J. Z., Ma Q. L., Ran F. R., Wang X. Z., Li H., Huang X., Xiong Q. H., Zhang Q., Gu L., Huang W., Zhang H., *Nat. Chem.*, **2018**, *10*, 638